Structural Modulation of Covalent Organic Frameworks for Efficient Hydrogen Peroxide Electrocatalysis

Rui Wang, Ziqi Zhang, Haiping Zhou, Mingrui Yu, Li Liao, Yan Wang, Sheng Wang, Haiyan Lu, Wei Xing, Valentin Valtchev, et al.

Structural Modulation of Covalent Organic Frameworks for Efficient Hydrogen Peroxide Electrocatalysis

Rui Wang,[+a] Ziqi Zhang,[+b] Haiping Zhou, [a] Mingrui Yu,[a,c] Li Liao,[d] Yan Wang,[a] Sheng Wan,[a] Haiyan Lu,*[a] Wei Xing,*[c] Valentin Valtchev,[e] Shilun Qiu,[a] and Qianrong Fang*[a]

[a] R. Wang, Y. Wang, H. Zhou, M. Yu, S. Wan, Prof. H. Lu, Prof. S. Qiu, Prof. Q. Fang
State Key Laboratory of Inorganic Synthesis and Preparative Chemistry,
Jilin University
Changchun 130012, R. P. China
E-mail: luhy@jlu.edu.cn (HL) or qrfang@jlu.edu.cn (QF)

[b] Z. Zhang
State Key Laboratory of Structural Chemistry
Fujian Institute of Research on the Structure of Matter, Chinese Academy of Sciences
Fuzhou 350002, China

[c] M. Yu, Prof. W. Xing
State Key Laboratory of Electroanalytical Chemistry, Laboratory of Advanced Power Sources Changchun
Institute of Applied Chemistry, Chinese Academy of Sciences
Changchun 130012, R. P. China
E-mail: xingwei@ciac.ac.cn (WX)

[d] Dr. L. Liao
School of Chemical Engineering and Technology,
Sun Yat-sen University,
Zhuhai 519082, P. R. China

[e] Prof. V. Valtchev
Qingdao Institute of Bioenergy and Bioprocess Technology, Chinese Academy of Sciences, Qingdao 266101, P. R. China;
Normandie Univ, ENSICAEN, UNICAEN, CNRS, Laboratoire Catalyse et Spectrochimie 6 Marechal Juin, 14050 Caen, France.

[+] These authors contributed equally to this work.

Supporting information for this article is given via a link at the end of the document.

Abstract: The electrochemical production of hydrogen peroxide (H_2O_2) using metal-free catalysts has emerged as a viable and sustainable alternative to the conventional anthraquinone process. However, the precise architectural design of these electrocatalysts poses a significant challenge, requiring intricate structural engineering to optimize electron transfer during the oxygen reduction reaction (ORR). Herein, we introduce a novel design of covalent organic frameworks (COFs) that effectively shift the ORR from a four-electron to a more advantageous two-electron pathway. Notably, the JUC-660 COF, with strategically charge-modified benzyl moieties, achieved a continuous high H_2O_2 yield of over 1200 mmol g^{-1} h^{-1} for an impressive duration of over 85 hours in a flow cell setting, marking it as one of the most efficient metal-free and non-pyrolyzed H_2O_2 electrocatalysts reported to date. Theoretical computations alongside in-situ infrared spectroscopy indicate that JUC-660 markedly diminishes the adsorption of the OOH* intermediate, thereby steering the ORR towards the desired pathway. Furthermore, the versatility of JUC-660 was demonstrated through its application in the electro-Fenton reaction, where it efficiently and rapidly removed aqueous contaminants. This work delineates a pioneering approach to altering the ORR pathway, ultimately paving the way for the development of highly effective metal-free H_2O_2 electrocatalysts.

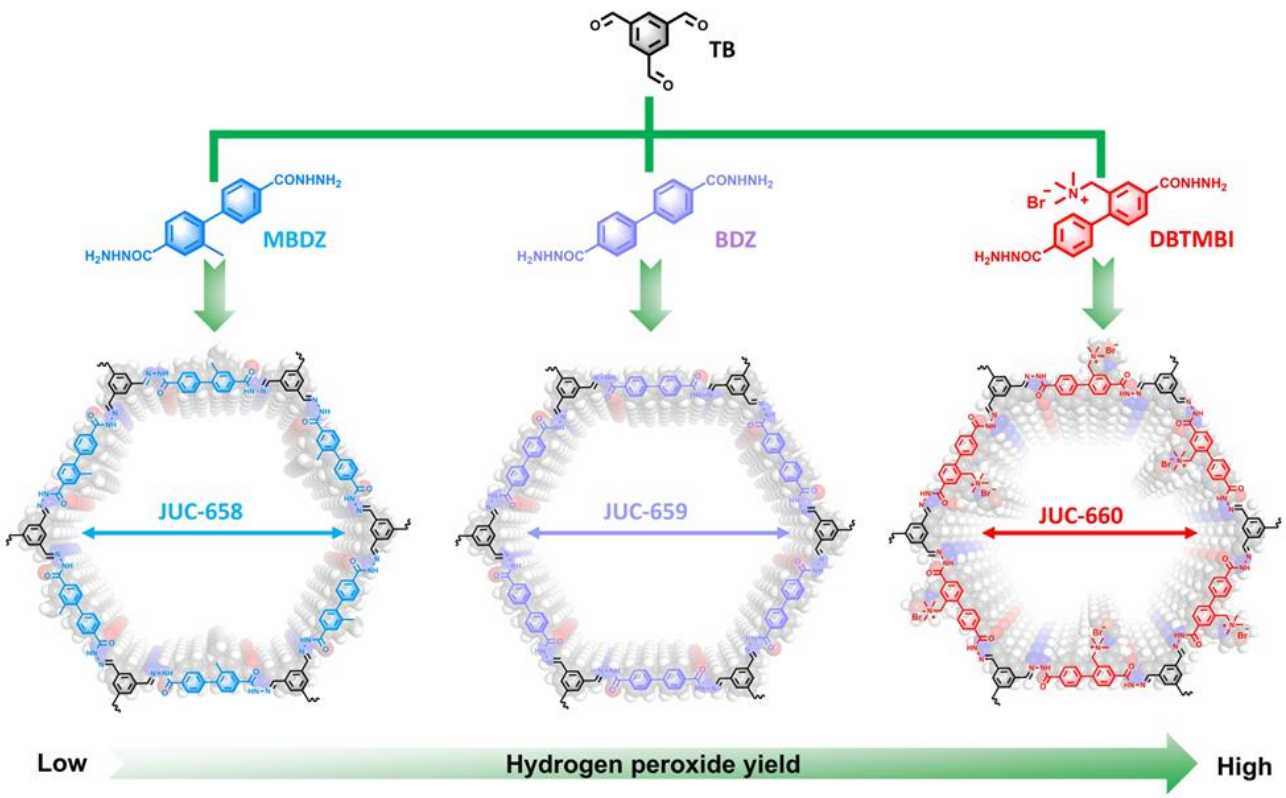

Scheme 1. Synthesis and structures of JUC-658, JUC-659, and JUC-660.

Hydrogen peroxide (H_2O_2) is recognized as one of the top 100 most indispensable chemicals globally due to its vital role across a diverse array of sectors such as paper production, textile manufacturing, and the realm of chemical synthesis.[1] Despite its widespread utility, the conventional industrial production of H_2O_2 via the anthraquinone process poses significant environmental concerns, encompassing the generation of considerable waste and the intensive energy requirements associated with its complex operations.[2] In light of these environmental implications, the electrosynthetic generation of H_2O_2, specifically through the oxygen reduction reaction (ORR) via a two-electron pathway, has garnered attention as a viable and sustainable alternative to the traditional anthraquinone method.[3] Although research has predominantly concentrated on metal-based catalysts within this domain[4], the rarity of specific metals and the negative externalities of their environmental footprint have constrained advancements.[5] Moreover, the catalytic sites of metals during H_2O_2 electrosynthesis can present deleterious effects.[6] An interesting turning point is that a series of metal-free carbon-based materials have shown effectiveness in the electro synthesis of H_2O_2, demonstrating the potential for a paradigm shift in this field.[7] However, these carbon materials generally require high-temperature pyrolysis to attain the necessary level of graphitization, which often results in poorly defined and erratic placement of active sites, posing a substantial obstacle to elucidating the structure-activity relationship in detail.[8] Consequently, developing metal-free catalysts for the electrosynthetic production of H_2O_2 that do not rely on pyrolysis and feature precisely characterized active sites alongside tunable structural properties is a critical challenge in contemporary research.[9]

Covalent organic frameworks (COFs), exemplified by their crystalline and porous nature, constitute an emergent class of materials crafted from light, non-metallic elements. They have received considerable interest for applications in electrocatalysis, attributable to their distinct features, including a well-defined structure, customizable catalytic active sites, and a porous framework.[10] Our recent work has developed a series of novel metal-free thiophene-S COFs, namely JUC-527 and JUC-528. These COFs exhibit enhanced ORR catalytic performance in an alkaline electrolyte compared to their thiophene-S-free counterparts, underscoring the effectiveness of pentacyclic thiophene-S moieties as potent active sites for ORR.[11] In a noteworthy study conducted in 2022, Wang and co-workers introduced BUCT-COF-11, a thiophene-enriched fully conjugated three-dimensional COF, synthesized using an all-thiophene-linked saddle-shaped constituent. This material has not only displayed exceptional semiconducting properties but has also demonstrated an inherent metal-free catalytic activity for ORR.[12] Despite these advancements, the majority of COF-based catalysts for ORR have primarily operated via a four-electron reaction pathway, which is less conducive to the generation of H_2O_2. Therefore, steering COF materials towards a two-electron reaction pathway represents a crucial strategy to

optimize the production of H_2O_2 and advance the field of COF-based electrocatalysis.[13]

organic polymers (COPs) have an inclination towards the two-electron process during ORR.[15] However, the amorphous

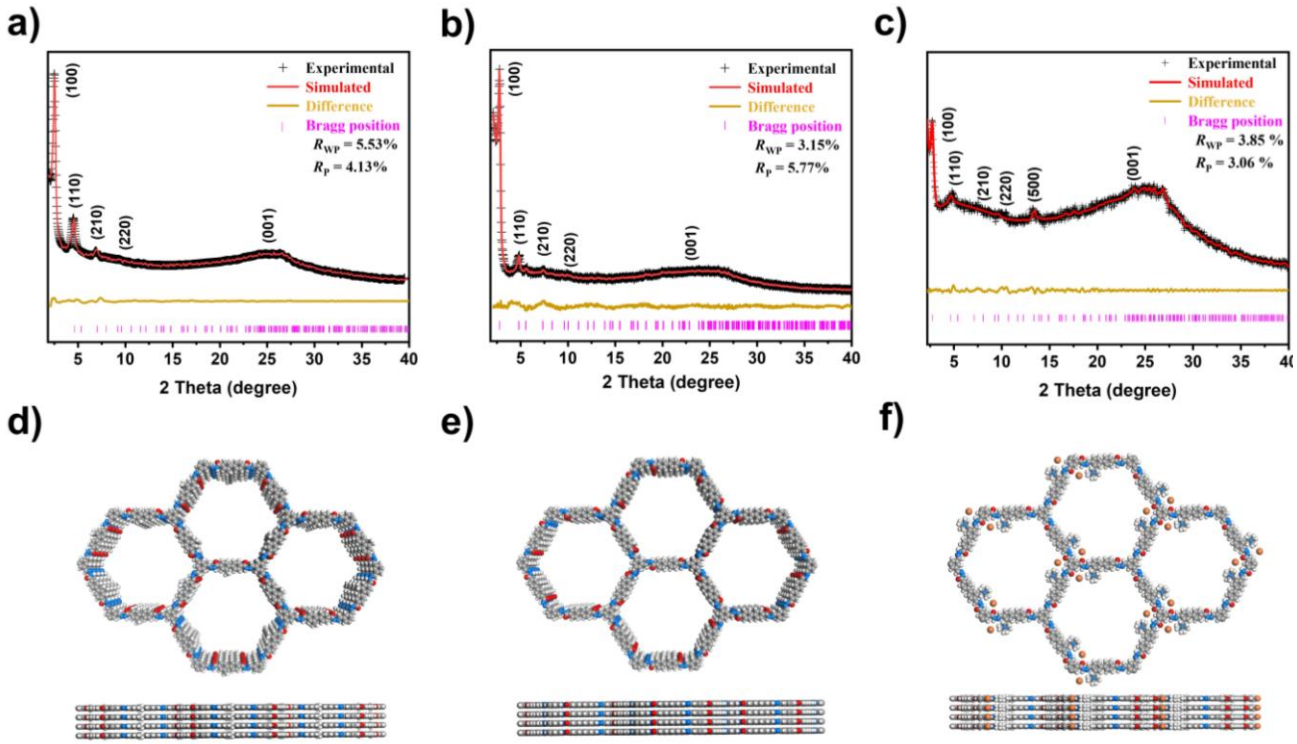

Figure 1. PXRD patterns of (a) JUC-658, (b) JUC-659, and (c) JUC-660. Observed patterns are shown in black, Pawley-refined patterns in red, the difference between observed and refined profiles in yellow, and Bragg positions in pink. Partial structures of JUC-658 (d), JUC-659 (e), and JUC-660 (f) are viewed along the *c*-axis and parallel to the *ab* plane. Atoms are represented as follows: C (gray), N (blue), O (red), Br (orange), and H (white).

In this study, we have successfully achieved a significant transformation from the traditional four-electron reaction pathway to the more targeted two-electron pathway, by incorporating a quaternary ammonium (QA) salt modification into a benzyl-functionalized COF, namely JUC-660. This alteration resulted in an impressive H_2O_2 conversion rate of up to 86.6%. To the best of our knowledge, this represents the inaugural instance of ionic COFs being employed for the electrosynthesis of H_2O_2. Moreover, when assembled into a flow-cell system, JUC-660 delivered a stable and robust performance, persisting more than 85 hours with a sustained yield rate exceeding 1200 mmol g^{-1} h^{-1}, a milestone that distinguishes it as one of significant advancement among the category of metal-free and non-pyrolyzed electrocatalysts. Comprehensive theoretical calculations in conjunction with in-situ infrared (IR) spectroscopy have revealed that the modification of the benzyl moiety with QA salts contributes to a decreased adsorption energy at the catalytic active site for the intermediate *OOH species, a pivotal factor in steering the ORR pathway. In addition, we demonstrated the practical utility of our innovative catalyst in conducting an electro-Fenton reaction, effectively degrading dyes in wastewater and illustrating its potential industrial applicability.

To achieve the objective of facilitating H_2O_2 electrosynthesis via a two-electron ORR pathway, our study focused on the development of ionic COFs. Prior investigations have suggested that charge-modified amorphous covalent nature of these materials obfuscates the precise understanding of their structure-activity relationships.[16] In contrast, the well-defined structures of ionic COFs offer not only the potential to favor the two-electron pathway in ORR but also to clarify structure-activity relationships with greater accuracy.[17] As a reference point for this progress, we designed and synthesized a trio of metal-free two-dimensional COFs with **hcb** structures using Schiff-base chemistry. As depicted in Scheme 1, we utilized 1,3,5-triformylbenzene (TB) as a linker to facilitate the formation of planar triangular units. Concurrently, three different linear building blocks were employed to construct the metal-free COFs: [1,1′-biphenyl]-4,4′-dicarboxylic acid dihydrazide (BDZ), 2-methyl-[1,1’-biphenyl]-4,4’-dicarbohydrazide (MBDZ), and 1-(4,4’-di(hydrazine carbonyl)-[1,1’-biphenyl]-2-yl)-N,N,N-trimethylmethanaminium (DBTMBI) for JUC-658, JUC-659, and JUC-660, respectively. Notably, JUC-660 was engineered through a bottom-up synthesis strategy, integrating a QA functional moiety that is essential in the formation of the anticipated ionic COF.

These COFs were synthesized through a solvothermal reaction in the presence of 6 M acetic acid for a duration of 7 days (Figure S1 and for detailed synthesis methods, please refer to the Supporting Information). Fourier-transform infrared (FT-IR) spectroscopy was employed to characterize their chemical structures. As shown in Figure S2, JUC-658 exhibited C=N stretching bands at 1671 cm^{-1}, JUC-659 at 1678 cm^{-1}, and JUC-660 at 1668 cm^{-1}, indicating the successful progression of the

Schiff-base reaction.[18] Furthermore, the disappearance of peaks at 1662 cm^{-1} related to C=O bonds, and 3197 cm^{-1}, 3194 cm^{-1}, and 3204 cm^{-1} for characteristic of N-H bonds, confirmed the advancement of the Schiff-reaction. Solid-state ^{13}C cross-polarization/magic-angle spinning (CP/MAS) nuclear magnetic resonance (NMR) spectra further validated the presence of characteristic C=N carbons, exhibiting peaks at 166 ppm for both JUC-658 and JUC-660, and 168 ppm for JUC-659 (see Figure S3).[19] Notably, JUC-660 displayed an additional peak at 52 ppm, attributed to the successful incorporation of the QA functional moieties within the COF.[20] Elemental analysis affirmed the presence of carbon, nitrogen, oxygen, and other elements in the synthesized COFs, closely aligning with the theoretical content (as shown in Table S1). X-ray photoelectron spectroscopy (XPS) was employed to monitor the electron density and chemical composition of three COFs. As shown in Figures S4-6, XPS spectra corroborated the presence of elements such as C, N, and O in these COFs. Additionally, the appearance of a 398.6 eV peak in Figure S6c reaffirmed the presence of QA functional moieties within JUC-660.[21]

The crystallinity of JUC-658, JUC-659, and JUC-660 was rigorously evaluated via powder X-ray diffraction (PXRD) patterns, which were further substantiated by structural simulations to affirm their respective crystalline architectures (refer to Figure 1 for PXRD patterns). Advanced computational simulations utilizing geometric energy minimization approaches were executed with Materials Studio package, specifically targeting the eclipsed hexagonal **hcb** network configuration. It was established that both JUC-658 and JUC-660 adopted a crystalline form within the *P*-6 space group symmetry (Space Group No. 174, as presented in Tables S2 and S4), while JUC-659 crystallized in the *P*6/m space group symmetry (Space Group No. 175, refer to Table S3). Notably, simulations demonstrated that all three COFs preferred an AA stacking sequence over AB, showcasing this arrangement in Figure S7. The unit cell parameters, generated from the simulation outputs, for each COF are as delineated: JUC-658 has lattice constants of $a = b = 38.5002$ Å and $c = 3.7052$ Å, with interaxial angles $\alpha = \beta = 90^{o}$ and $\gamma = 120^{o}$; JUC-659 has dimensions $a = b = 38.2343$ Å and $c = 3.4374$ Å, accompanied by identical interaxial angles; JUC-660 displays $a = b = 38.3783$ Å and $c = 3.9332$ Å with congruent interaxial angles as the former two. These simulated lattice parameters are in exceptional agreement with the respective empirical measurements. Experimentally, JUC-658 exhibited distinctive diffraction peaks at 2θ values of 2.69, 4.64, 7.08, 9.87, and 24.69 degrees, assignable to the (100), (110), (210), (220), and (001) crystal planes, respectively. Parallel observations were made for JUC-659, with peaks occurring at $2\theta = 2.63$, 4.59, 6.98, 9.83, and 23.54 degrees, and JUC-660 with comparable peaks at 2.67, 4.62, 7.03, 9.85, and 24.71 degrees. Significantly, these diffraction positions correlated with the calculated planes. To enhance the validity of the PXRD data, a full profile pattern matching (Pawley fitting) refinement was employed, indicating precise agreement between the refined and experimental profiles. The refinement metrics demonstrated outstanding data congruency, with negligible discrepancies and superior fit quality (with JUC-658, $R_p = 4.13\%$ and $R_{wp} = 5.53\%$; JUC-659, $R_p = 5.77\%$ and $R_{wp} = 3.15\%$; JUC-660, $R_p = 3.77\%$ and $R_{wp} = 4.78\%$).

The porosity of these COFs was quantitatively characterized through the analysis of N_2 adsorption-desorption isotherms at 77 K, documented in Figure S8. The isotherms for each material displayed the archetypal Type IV behavior, indicative of mesoporous structures—a key point emphasized by standardized IUPAC classification.[22] A pronounced adsorption uptake was observed when the relative pressure P/P_0 was less than 0.1, proceeding with inflection steps around P/P_0 values of 0.15 or 0.25. Utilizing the Brunauer-Emmett-Teller (BET) theory, the specific surface areas of the COFs were calculated to be 302 $m^2\ g^{-1}$ for JUC-658, 338 $m^2\ g^{-1}$ for JUC-659, and 226 $m^2\ g^{-1}$ for JUC-660, respectively. The comparatively reduced surface area of JUC-660 can be attributed to the incorporation of QA functional moieties, which are known to impact crystallinity through electrostatic interactions, as posited in previous research.[23] Additionally, a conspicuous hysteresis loop in the N_2 adsorption-desorption isotherm of JUC-660 was noted (please refer to Figure S8g), suggesting possible ion-dipole interactions between nitrogen molecules and the QA functional moieties intrinsic to the framework.[24] Pore size distributions derived from the Barret-Joyner-Halenda (BJH) method revealed the existence of a monodisperse pore diameter within each COF—namely 36.6 Å for JUC-658 (Figure S8c), 38.7 Å for JUC-659 (Figure S8f), and 31.4 Å for JUC-660 (Figure S8i). These experimentally determined values show remarkable concordance with their respective simulated structural counterparts (39.2 Å for JUC-658, 40.0 Å for JUC-659, and 34.4 Å for JUC-660).

Thermogravimetric analysis (TGA) conducted under an inert nitrogen atmosphere revealed nominal weight loss at temperatures below 250 °C (as detailed in Figure S9). Mass reductions observed below 100°C can be largely attributed to the evaporation of water molecules previously adsorbed within the pores of the COFs. To critically evaluate their chemical resilience, these COFs underwent rigorous exposure to a battery of chemical solvents—including toluene, tetrahydrofuran, acetone, and n-hexane—over a duration of three days. Post-exposure analysis indicated that their crystalline structures remained intact with no discernible changes, attesting to their robustness (refer to Figure S10a-c for detailed structural analysis). Furthermore, the integrity of all three COFs was put to the test in both basic (0.1 M KOH aqueous solution) and acidic (0.05 M H_2SO_4 aqueous solution) environments over an extended period of three days. Despite these challenging conditions, they displayed commendable chemical sturdiness, maintaining their crystallographic and structural soundness—a prime indicator of their viability for ORR applications, as documented in Figure S10d-f.

The surface morphologies of the trio of COFs were meticulously examined via scanning electron microscopy (SEM). Figure S11 evidences that JUC-658 and JUC-659 both exhibit spheroidal morphologies adorned with flower-like structures, whereas JUC-660 is characterized by a distinct lamellar topology. Complementary insights were garnered through transmission electron microscopy (TEM), which unveiled a consistent lamellar architecture across all three COFs, with an

estimated diameter of 100 nanometers (as presented in Figure S12). Spectroscopic analysis—specifically energy-dispersive X-ray spectroscopy (EDS), was utilized to elucidate the elemental makeup of these materials. Figures S13-15 depict a homogeneous distribution of carbon, nitrogen, and oxygen elements within each of the COFs. Notably, in JUC-660, bromine was also detected and was found to be uniformly dispersed, thereby corroborating the findings obtained from X-ray photoelectron spectroscopy (XPS) and elemental analyses. Furthermore, the wettability of these materials—a critical factor influencing their potential utility as heterogeneous catalysts in aqueous systems—was quantified through contact angle measurements (Figure S16). The resultant values were 44.2° for JUC-658, 28.6° for JUC-659, and a notably lower 16.3° for JUC-660. Lower contact angles suggest a higher affinity for aqueous environments, a desirable trait for heterogeneous catalysis within such phases.[21]

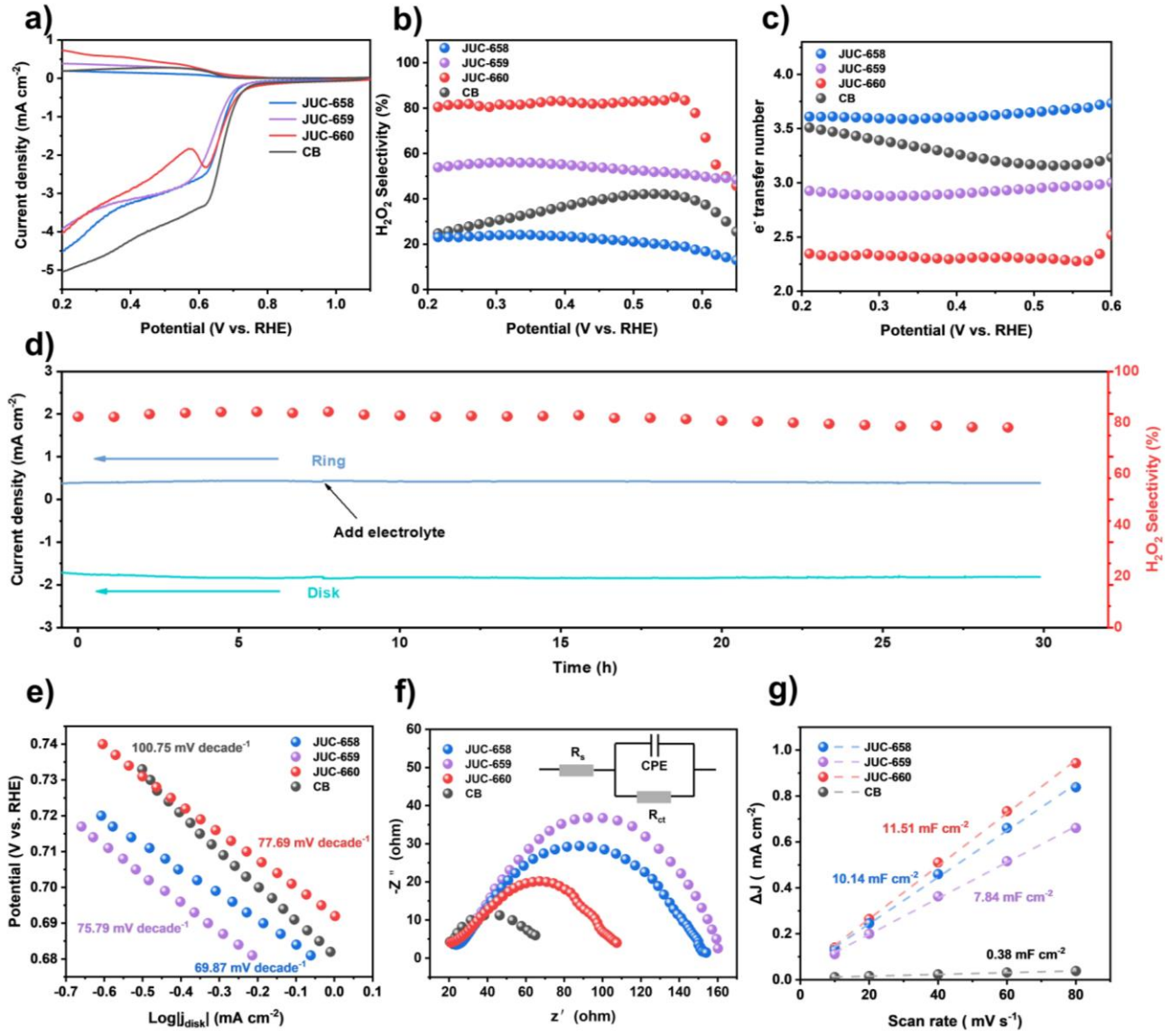

Figure 2. (a) LSV curves of JUC-658, JUC-659, JUC-660, and carbon black in O_2-saturated 0.1 M KOH electrolyte. (b) The corresponding H_2O_2 selectivity and (c) electron transfer number of JUC-658 (blue), JUC-659 (purple), JUC-660 (red), and carbon black (black) calculated from RRDE results in O_2-saturated 0.1 M KOH. (d) Stability tests of JUC-660 at a potential of 0.57 V vs RHE in O_2-saturated 0.1 M KOH. (e) The corresponding Tafel slopes of JUC-658 (blue), JUC-659 (purple), JUC-660 (red), and carbon black (black) in O_2-saturated 0.1 M KOH. (f) Impedance measurements for JUC-658 (blue), JUC-659 (purple), JUC-660 (red), and carbon black (black) in O_2-saturated 0.1 M KOH. Inset: the equivalent electric circuit. (g) Cdl measurements of JUC-658 (blue), JUC-659 (purple), JUC-660 (red), and carbon black (black) in O_2-saturated 0.1 M KOH.

To thoroughly evaluate the electrocatalytic capabilities of the three COFs in the ORR within a 0.1 M KOH electrolyte, a conventional three-electrode system integrated with a rotating ring-disk electrode (RRDE) apparatus was employed. The collection efficiency of this setup, based on the redox conversion of $[Fe(CN)_6]^{4-}$/ $[Fe(CN)_6]^{3-}$, was determined to be around 0.38. Subsequent a collection of linear sweep voltammetry (LSV) profiles was performed at a consistent rotational velocity of 1600 revolutions per minute, which can be referred to in Figure S17. Further methodological specifics are delineated within the Supplementary Information section. Acknowledging the intrinsically low conductive properties of COFs, it is a standard practice to incorporate conductive carbon black as a dopant to augment the electrical conductivity of the COF substrates. This scheme is prevalently applied to metal-free and non-pyrolyzed COF catalysts.[25] As depicted in Figure 2a, the assessed COFs demonstrated comparable onset potentials (0.774 V for JUC-658, 0.763 V for JUC-659, and 0.869 V for JUC-660) alongside their respective half-wave potentials (0.62 V for JUC-658, 0.59 V for JUC-659, and 0.64 V for JUC-660). While the disk current densities appeared analogous among the COFs, contrasting ring current densities noted indicated a disparity in electron transfer rates.[26] Using RRDE data, the electron transfer numbers (n) and subsequent H_2O_2 selectivity percentages for the COFs and conductive carbon blacks were extrapolated. Figure 2b and 2c depict the H_2O_2 generation and electron transfer metrics

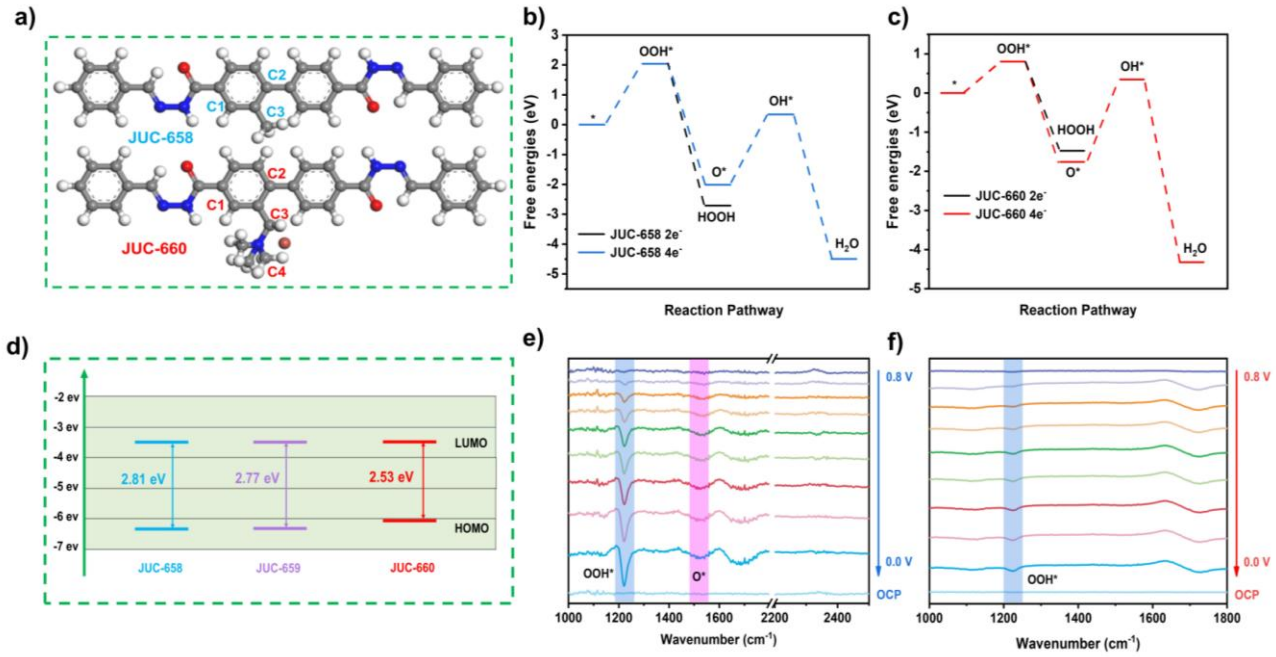

Figure 3. (a) Predicted active sites of JUC-658 and JUC-660 molecular fragment. (b) Free energy diagram for JUC-658 for two-electron pathway and four-electron pathway. (c) Free energy diagram for JUC-660 for two-electron pathway and four-electron pathway. (d) Energy level diagram of the JUC-658, JUC-659, and JUC-660. In-situ FT-IR spectra of JUC-658 (e) and JUC-660 (f).

throughout a potential range of 0.20 V to 0.60 V vs. RHE. JUC-658 was characterized by a H_2O_2 yield ranging from 16% to 22% and an electron transfer number oscillating between 3.6 and 3.7. JUC-659 yielded 49% to 55% H_2O_2 with its electron transfer number spanning from 2.9 to 3.1. JUC-660, on the other hand, showcased superior H_2O_2 yields of 81% to 86% with an associated electron transfer number of approximately 2.2 to 2.4. These findings imply that the catalytic reaction mechanisms of these materials approximate towards the four-electron transfer pathway, the mixed "three-electron transfer pathway" (where two- and four-electron pathways are comparable), and the two-electron transfer pathway, respectively.

Additionally, the numbers of electron transfer for JUC-658, JUC-659, JUC-660, and conductive carbon black were determined by employing the Koutecký–Levich (K–L) equations at an applied potential of 0.2 V vs. RHE, yielding values of 3.47, 3.04, 2.49, and 2.97, respectively, as illustrated in Figure S18. These values corroborate with those derived from the RRDE methodologies. In the context of H_2O_2 electrosynthesis via the ORR, the quad-electron pathway is less desirable since it predominantly yields H_2O as the product.[27] With JUC-660's distinguished H_2O_2 selectivity, its stability was also evaluated, which is imperative for its overall catalyst efficacy.[28] After 30 hours of unrelenting assessment at 0.57 V—a potential where JUC-660 culminated in an H_2O_2 selectivity peaking at approximately 86%—the selectivity steadfastly remained over 78%, underscoring the catalyst's substantial stability in 0.1 M KOH (refer to Figure 2d).

The mass activity of three COF catalysts and conductive carbon black at varied operating potentials was quantified as well (refer to Figure S19). Remarkably, JUC-660 reached a mass activity apex of 3.66 A g^{-1} concomitant with its highest H_2O_2 selectivity at 0.57 V. In comparison, JUC-658 exhibited a mass activity of 4.36 A g^{-1}, concurrent with optimal water production selectivity at 0.6 V. Turnover frequencies (TOF) of JUC-658 and JUC-660 at divergent potentials were computed too (refer to Figure S20). At 0.57 V, JUC-660 demonstrated a TOF of 0.069 s^{-1}, while JUC-658 evinced a TOF of 0.037 s^{-1} at 0.6 V.

Tafel plots, extrapolated from the LSV data gathered using a disk electrode, are displayed in Figure 2e. Therein, JUC-658, JUC-659, and JUC-660 manifest Tafel slopes of 69.87 mV dec^{-1}, 75.79 mV dec^{-1}, and 77.69 mV dec^{-1}, respectively—an indication of more rapid kinetic process in ORR relative to conductive carbon blacks, which exhibited a greater slope of 100.75 mV dec^{-1}.[29] Furthermore, to scrutinize the materials under ORR conditions, electrochemical impedance spectroscopy (EIS) measurements were instigated at the potential of 0.8 V (vs. RHE) in 0.1 M O_2-saturated KOH solution by applying an AC voltage with an amplitude of 5 mV and a frequency range of 10^5-10^{-1} Hz. The findings revealed a diminution in the interfacial charge transfer resistance of JUC-660 in comparison to JUC-658 and JUC-659, albeit it remained superior to conductive carbon black. An equivalent circuit model, framed to simulate the EIS outcomes, is delineated in Figure 2f. In addition, we conducted additional experiments using the spin coating method at 800 rpm to prepare the samples. The impedance results obtained from the spin coating method were consistent with those from the drop casting method, thereby validating the reliability of the drop casting method for our systematic impedance comparison (Figure S21 and Table S5).

The electrochemically active surface area (ECSA) of the trio of COFs, alongside conductive carbon blacks, was meticulously assessed using cyclic voltammetry (CV) within the non-faradaic

potential range of 0.90-1.10 V vs. RHE. These measurements were conducted at scan rates ranging from 10 to 80 mV s^{-1} in a 0.1 M KOH electrolyte and have been depicted in Figure S22.[30] It was quite remarkable to observe that the double-layer capacitance (Cdl) for JUC-660 and JUC-658 exhibited comparable values, attaining 11.51 mF cm^{-2} and 10.14 mF cm^{-2}, respectively. These values were notably superior to that of JUC-659, which was recorded at 7.84 mF cm^{-2}. In comparison, the original conductive carbon black possessed a significantly higher Cdl (0.38 mF cm^{-2}). This elevated Cdl, coupled with a vast pore structure, synergistically enhance electrolyte diffusion. Such facilitation of electrolytic movement permits the electrode surface to accrue a higher quantity of reactant intermediates from the electrolyte. Consequently, this culminates in an augmented ORR performance.[31]

To comprehend the divergent catalytic product profiles of JUC-658 and JUC-660, it is imperative to first delineate the active sites within these catalysts. It is noteworthy that recent work has indicated that a series of methyl-modified metal-free COFs have an ortho activation effect, modulating the adjacent carbon atom as the catalytic active site.[14] Therefore, considering the potential active sites on the side chains, we employed density functional theory (DFT) calculations in Vienna ab initio simulation (VASP) package to explore the active sites of these catalysts based on the optimized model molecular units. The potential active sites are labelled in Figure 3a, and the possible theoretical adsorption models are shown in Figures S23-29. The adsorption energies for the intermediates in the two-electron and four-electron ORR were calculated at these potential sites. These calculated energies for JUC-658 and JUC-660 are systematically compiled in Tables S6 and S7, respectively. Figure S30b presents the intermediate adsorption energies for the four-electron process across four different sites, while Figure S30a does the same for the two- electron process. These energies reveal that for JUC-658, the C1 site exhibits the lowest adsorption energy in the four-electron process, whereas for JUC-660, the C1 site shows the lowest adsorption energy (-1.48 eV) for intermediates in the two-electron process, hence identifying the C1 site as the primary active center in both COFs. Delving further, as depicted in Figure 3b and 3c, the intermediate peroxide (OOH*) adsorption energy at the C1 site for JUC-658 was higher than that for JUC-660, indicating a modulation of adsorption capacity at the C1 site as a consequence of a QA moiety introduction in JUC-660, and an amplification due to a methylene functional moiety in JUC-658. The reason for this change in adsorption energy may be due to the redistribution of charge on the COF due to the introduction of the QA moiety.[32] This differential in adsorption behavior aids the easier release of OOH* from JUC-660's C1 site, promoting the protonation of solvated species to generate H_2O_2. In contrast, JUC-658 retains OOH* at the C1 site with greater affinity, thereby favoring the progression to the subsequent O* intermediate. That is, JUC-660 has more thermodynamically favorable two-electron ORR properties than JUC-658. These assertions are substantiated through in-situ IR spectroscopy, with Figure 3e and 3f delineating the spectral changes at varying voltages. For JUC-660, the OOH* peak intensity is diminished relative to JUC-658, whereas the formation of the O* intermediate is clearly discernible in JUC-658's spectrum, a feature absents in JUC-660's spectroscopic profile. This contrast reinforces the distinct ORR mechanisms between the two COFs. This comparison emphasizes the existence of distinct ORR mechanisms when two COFs are employed as electrocatalysts. The density of states (DOS) plots of the different elements of JUC-658 and JUC-660 are also shown in Figure S31.

Furthermore, the optical bandgaps of JUC-658, JUC-659, and JUC-660 were ascertained through the application of the Kubelka-Munk function.[33] The findings delineated that JUC-658 and JUC-659 possess similar optical bandgaps of 2.81 eV and 2.77 eV, respectively. Notably, JUC-660 exhibits a reduced optical bandgap of 2.53 eV, which is documented in Figures 3d and S32. Additionally, the energetic parameters concerning the highest occupied molecular orbital (HOMO) and the lowest unoccupied molecular orbital (LUMO) for these COFs were estimated. Through the use of CV techniques, the HOMO and LUMO energy levels were established, consequently highlighting the semiconductive nature of these COFs.[34] These electronic properties are elaborated upon in Figures S33 and S34 of the

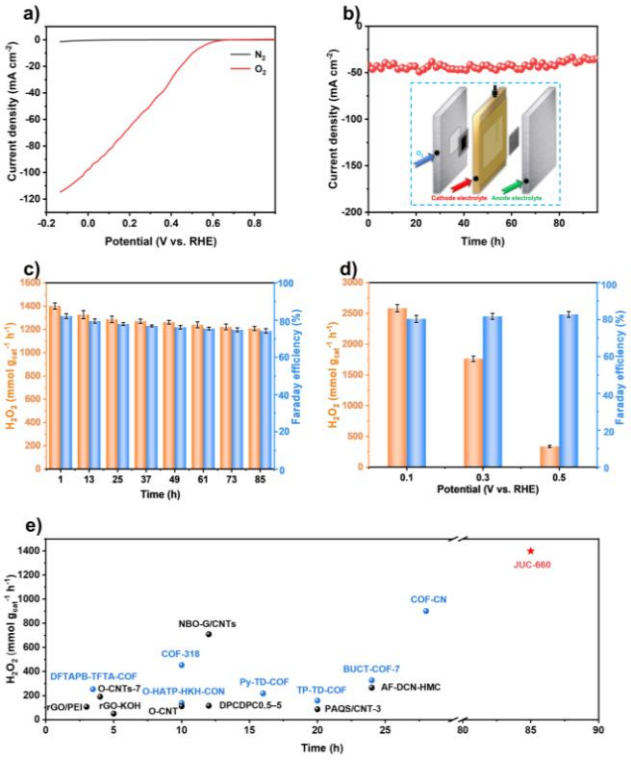

Figure 4. (a) LSV curves of JUC-660 are introduced into the flow cell with oxygen and nitrogen in 0.1 M KOH, respectively. (b) The stability curve of the flow cell in 0.1 M KOH. Inset: schematic diagram of the flow cell structure. (c) H_2O_2 yield rates and Faraday efficiency in 0.1 M KOH over time during the stability test time. (d) Faraday efficiency and H_2O_2 yield rates at 0.1 V, 0.3 V and 0.5 V (vs. RHE) during 1 hour in 0.1 M KOH. (e) Comparison of the H_2O_2 yield rate and stability of JUC-660 with the currently known metal-free and non-pyrolyzed catalysts under analogous conditions.

Supporting Information.

Following the confirmation of JUC-660's outstanding selectivity for H_2O_2 production, the catalyst was incorporated within a flow cell to appraise its intrinsic capability for oxygen generation under high current densities. All experimental data of the flow cell were tested in triplicate trials to reduce possible errors during the experiment. The construction details of the flow cell are meticulously described in the supplementary information and illustrated in Figures S35 and 4b. Performance characteristics are captured in Figure 4a, which presents the LSV profiles of the flow cell within both nitrogen and oxygenated environments. Remarkably, a current density exceeding 100 mA cm^{-2} is observed when the cell is oxygenated, whereas the current density plummets to nearly 0 mA cm^{-2} under a nitrogen blanket, suggesting an absence of reaction in inert conditions. In order to further substantiate the exceptional catalytic activity of JUC-660, a baseline measurement was conducted using a gas diffusion electrode in the absence of the catalyst coating, serving as a control within the flow cell. The observed current density in this control setup was close to 0 mA cm^{-2}, as evidenced in Figure S36. This control experiment reaffirms the superior catalytic efficacy of JUC-660 in facilitating the electrochemical production process.

The robustness of any catalyst utilized in the electro-synthetic production of H_2O_2 is of paramount importance. As depicted in Figure 4b, JUC-660 showcases extraordinary stability, enduring continuous operation for an extended period, nearly four days, at elevated current densities in excess of 40 mA cm^{-2}. Throughout the course of stability testing, the H_2O_2 generation rates and FE were precisely quantified via a universal cerium sulfate titration technique, calibrated against a pre-established standard curve (Figure S37). Data presented in Figure 4c elucidates the H_2O_2 production rate and FE associated with the JUC-660 apparatus. A delineation of the results, especially from Figure 3c, reveals a gradual diminution in both the yield rates of H_2O_2 and FE over the test duration. Significantly, initial measurements within the first hour show H_2O_2 yield rates peaking at 1398 mmol g^{-1} h^{-1} and FE reaching 83.6%. After 85 hours of consistent operation, we have tested UV-vis spectra of Ce^{4+} solutions of cathode electrolytes at different times and different voltages (Figures S40 and S41), and the rate of hydrogen peroxide generation and Faraday efficiency can be calculated with a considerable H_2O_2 production rate of approximately 1213 mmol g^{-1} h^{-1} and an FE of around 76%. A further series of tests were conducted to ascertain the H_2O_2 yields and FE at variable potentials; the findings outlined in Figure 4d demonstrate diverse outcomes. At a potential of 0.1 V, the H_2O_2 yield was 1864 mmol g^{-1} h^{-1}, with an FE of 82.2%. At 0.3 V, yield declined to 1241 mmol g^{-1} h^{-1} with a slightly improved FE of 83.8%, and at 0.5 V, the yield plunged to 334 mmol g^{-1} h^{-1}, yet with the highest recorded FE of 84.4%. Comparative analyses featured in Figure 4e assess the JUC-660 against alternative metal-free and non-pyrolyzed catalysts under analogous conditions, such as a yield of 901 mmol g^{-1} h^{-1} with a durability of 28 hours for COF-CN,[32] a yield of 709 mmol g^{-1} h^{-1} with a lifetime of 12 hours for NBO-G/CNTs, [35] and a yield of 50 mmol g^{-1} h^{-1} sustained over 5 hours for rGO-KOH.[36] JUC-660's superior performance exceeds these counterparts, establishing it as one of the preeminent metal- and pyrolysis-free electrocatalyst thus far reported (Table S8).

In order to verify that the JUC-660 has perfect reproducibility, two additional long-term stability tests of the three-phase flow cell were also performed (Figure S42). In addition, the LSV curve of JUC-660 was measured after long-term stability. As shown in Figure S43, there is not much change from before the test. The pH changes of the electrolyte were monitored throughout the electrosynthesis of H_2O_2. As shown in Figure S44, the pH of the electrolyte remained nearly constant, exhibiting only minor fluctuations over time. Despite the different half-reactions occurring at the cathode and anode, the permeation of OH^- ions through the AEM helps maintain a stable pH in both chambers. This stability is crucial for the efficient and consistent production of H_2O_2 over extended reaction periods. We also conducted additional characterizations, including SEM, TEM, XPS, and EDS, on JUC-660 after long-term tests (Figures S45-50). SEM and TEM images indicate that the JUC-660 electrocatalyst underwent electrochemical exfoliation, a phenomenon commonly observed in two-dimensional materials.[37] The XPS and EDS data show no significant changes before and after the long-term stability test, suggesting that the microstructure of JUC-660 are retained. We could not obtain PXRD data for JUC-660 after long-term tests due to the exfoliation of the sample and the introduction of amorphous carbon powder during sample preparation.

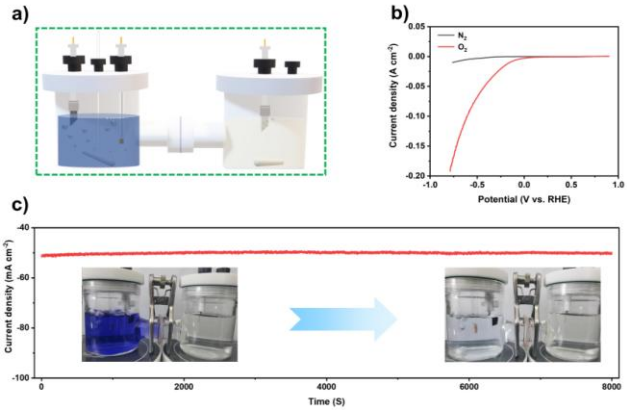

Figure 5. (a) Schematic diagram of an H-type electrolytic cell used for an Electro-Fenton reaction. (b) LSV curves of H-type electrolytic cell in nitrogen and oxygen atmospheres in O_2-saturated 0.5 M H_2SO_4. (c) Stability curves in in O_2-saturated 0.5 M H_2SO_4 during an electro-Fenton reaction. Inset: Change in the color of the cathode of the H-cell before and after the electro-Fenton reaction.

Moreover, the proficiency of JUC-660 in the electro-synthesis of H_2O_2 was scrutinized under acidic conditions (0.5 M H_2SO_4) using an H-shaped electrolytic cell. Figure 5a reveals the arrangement, wherein the synthesized JUC-660 catalyst was coated onto a hydrophilic carbon paper and installed within the cell. The cell was designed to contain electrolytes on each side, partitioned by a cation exchange membrane to avoid cross-mixing. To evaluate the oxygen reduction capabilities of the catalyst under acidic conditions, LSV measurements were

carried out in both O_2-saturated and N_2-saturated sulfuric acid solutions. The data showcased in Figure 5b points to the outstanding oxygen reduction prowess of JUC-660 in an acidic milieu. Additionally, the result corroborates that the catalyst attains a notable current density of nearly 200 mA cm^{-2} at a potential of -0.8 V. Notably, at such negative potentials, it is essential to account for the influence of the hydrogen evolution reaction (HER).[38] To this end, the HER performance was also charted. The outcomes distinctly demonstrate that JUC-660 possesses a significant suppressive impact on the HER. This quality is notably advantageous for the acidic ORR occurring concurrently at the same potential as it heightens the FE of the ORR, thereby improving the overall catalytic efficiency of the process.[39]

The electro-Fenton reaction is integral to advancing water purification techniques, with the in-situ electro-synthesis of H_2O_2 under acidic conditions being a key component in facilitating this reaction.[40] The remarkable efficacy of JUC-660 in the electro-synthesis of H_2O_2 suggests its potential as a superior electro-Fenton catalyst, particularly for the degradation of organic dye pollutants in acidic media. Subsequently, a high-concentration solution of Coomassie Brilliant Blue (200 ppm) was employed as a representative dye contaminant. As evidenced in Figure 5c, there is a near-complete degradation of the dye within 8000 seconds. Visual confirmation of this degradation is provided in the inset of Figure 5c, where a progressive fading from deep blue to a colorless state is observed. The versatility of JUC-660 was further evaluated using additional dye contaminants, namely Rhodamine B and the ionic dye Fluorescein sodium, each at lower concentrations of 10 ppm. The results, depicted in Figures S51 and S52, indicate a swift degradation of both dyes within just five minutes. The efficiency of the degradation processes was quantitatively discerned through UV-spectrophotometric analysis, showcased in Figure S53, where the characteristic absorption peaks of the dyes were nearly undetectable post-treatment. This rapid and effective degradation highlights the catalytic prowess of JUC-660 and its potential application in water treatment technologies.

In summary, we achieved a significant alteration from a four-electron process to a two-electron process in the ORR process by strategically structural modulation of the QA salt moiety within the COFs. The JUC-660 catalyst demonstrated exceptional selectivity, achieving an 86.6% yield in the electro-synthesis of H_2O_2. When integrated into a JUC-660-based flow cell, the system delivered impressive yield rates and stability for H_2O_2, maintaining continuous operation for more than 85 hours with a yield exceeding 1200 mmol g^{-1} h^{-1}. Such performance metrics position our catalyst at one of the forefront of known metal-free and non-pyrolyzed electrocatalysts. The efficiency of this modification was reinforced by in-situ IR spectroscopic analysis and corroborated by theoretical simulations. Additionally, the application of this catalyst in the electro-Fenton reaction has proven to be fruitful, demonstrating the rapid decolorization of dyes from aqueous solutions within a brief duration. This research not only offers a viable strategy to modulate the electron transfer in ORR but also establishes a foundational approach for the design and development of highly proficient electrocatalysts, characterized by their precision and the capacity for manipulation at the active sites.

Conflict of interest

The authors declare no conflict of interest.

Acknowledgements

This work was supported by National Key R&D Program of China (2021YFF0500504 and 2022YFB3704900), National Natural Science Foundation of China (22025504, 21621001, and 22105082), the SINOPEC Research Institute of Petroleum Processing, "111" Center (BP0719036 and B17020), China Postdoctoral Science Foundation (BX20230143, 2020TQ0118 and 2020M681034), and the program for JLU Science and Technology Innovative Research Team. V.V., Q.F. and S.Q. acknowledge the collaboration in the framework of China-French research network "Zeolites". Super-computing facilities were provided by the Hefei Advanced Computing Center.

Keywords: Covalent organic frameworks • Hydrogen peroxide production • Oxygen reduction reaction • Metal-free catalysts • Electrocatalysis

[1] a) W. Zhao, P. Yan, B. Li, M. Bahri, L. Liu, X. Zhou, R. Clowes, N. D. Browning, Y. Wu, J. W. Ward, and A. I. Cooper, *J. Am. Chem. Soc.* **2022**, *144*, 9902−9909; b) S. Siahrostami, S. Villegas, A. Mostaghimi, S. Back, A. Farimani, H. Wang, K. A. Persson and J. Montoya, *ACS Catal.* **2020**, *10*, 7495−7511.

[2] a) J. Lim, J. Kim, J. Woo, T. Shin, Y. Sa and S. Joo, *Chem* **2021**, *7*, 3114–3130; b) P. Das, G. Chakraborty, J. Roeser, S. Vogl, J. Rabeah, and A. Thomas, *J. Am. Chem. Soc.* **2023**, *145*, 2975−2984.

[3] a) X. Yang, Y. Zeng, W. Alnoush, Y. Hou, D. Higgins and G. Wu, *Adv. Mater.* **2022**, *34*, 2107954; b) X. Li, Q. Liu, B. Yang, Z. Liao, W. Yan, and Z. Xiang, *Adv. Mater.* **2022**, *34*, 2204570.

[4] a) M. Song, W. Liu, J. Zhang, C. Zhang, X. Huang and D. Wang, *Adv. Funct. Mater.* **2023**, *33*, 2212087; b) R. Wang, J. Zhao, Q. Fang, S. Qiu, *Chem. Synth.* **2024**, *4*, DOI: 10.20517/cs.2023.61.

[5] Y. Lin, H. Kuang, S. Zhang, X. Zhang, G. Zhai, X. Lin, D. Xu, J. Jia, X. Li and J. Chen, *CCS Chem.* **2022**, *4*, 3482–3490.

[6] a) M. Bhatt and J. Lee, Energy Fuels **2020**, *34*, 6634−6695; b) J. Liu, Z. Gong, M. Yan, G. He, H. Gong, G. Ye and H. Fei, *Small* **2022**, *18*, 2103824.

[7] N. Wang, S. Ma, P. Zuo, J. Duan, and B. Hou, *Adv. Sci.* **2021**, *8*, 2100076.

[8] X. Cui, L. K. Gao, R. Ma, Z. N. Wei, C. H. Lu, Z. L. Li, Y. K. Yang, *J. Mater. Chem. A* **2021**, *9*, 20985.

[9] M. M. Fernández, E. M. Periñán, A. P. Ruigómez, J. J. Cabrera-Trujillo, J. A. R. Navarro, F. A. Galindo, D. R. S. Miguel, M. Ramos, R. Vismara, F. Zamora, E. Lorenzo and J. L. Segura, *Angew Chem. Int. Ed.* **2023**, *62*, e202313940.

[10] a) Y. Liu, C. Wu, Q. Sun, F. Hu, Q. Pan, J. Sun, Y. Jin, Z. Li, W. Zhang and Y. Zhao, *CCS Chem.* **2020**, *2*, 2418–2427; b) C. Ji, C. Kang, B. Patra and D. Zhao, *CCS Chem.* **2023**, DOI: 10.31635/ccschem.

023.202303415; c) X. Yin, Y. Hua and Z. Gao, *CCS Chem.* **2023**, DOI: 10.31635/renewables.023.202200003; d) J. Zhou and Bo Wang, *Chem. Soc. Rev.* **2017**, *46*, 6927.

[11] D. Li, C. Li, L. Zhang, H. Li, L. Zhu, D. Yang, Q. Fang, S. Qiu, and X. Yao, *J. Am. Chem. Soc.* **2020**, *142*, 8104−8108.

[12] R. Bao, Z. Xiang, Z. Qiao, Y. Yang, Y. Zhang, D. Cao and S. Wang, *Angew. Chem. Int. Ed.* **2023**, *62*, e202216751.

[13] H. Zhang, M. Zhu, O. G. Schmidt, S. Chen and K. Zhang, *Adv. Energy Sustainability Res.* **2021**, *2*, 2000090.

[14] Z. You, B. Wang, Z. Zhao, Q. Zhang, W. Song, C. Zhang, X. Long and Y. Xia, *Adv. Mater.* **2023**, *35*, e2209129.

[15] a) W. Li, Z. Zhao, W. Hu, Q. Cheng, L. Yang, Z. Hu, Y. A. Liu, K. Wen and H. Yang, *Chem. Mater.* **2020**, *32*, 8553–8560; b) L. Peng, P. Liu, Q. Cheng, W. Hu, Y. A. Liu, J. Li, B. Jiang, X. Jia, H. Yang and K. Wen, *Chem.Commun.* **2018**, *54*, 4433-4436.

[16] a) W. Zhang, L. Zhou, Y. Shi, Y. Liu, H. Xu, X. Yan, Y. Zhao, Y. Jiang, J. Zhang, and Z. Gu, *Angew. Chem. Int. Ed.* **2023**, *62*, e202304412; b) S. Mondal, B. Mohanty, M. Nurhuda, S. Dalapati, R. Jana, M. Addicoat, A. Datta, B. K. Jena, and A. Bhaumik, *ACS Catal.* **2020**, *10*, 5623; c) C. H. Yang, Z. D. Yang, H. Dong, N. Sun, Y. Lu, F. Zhang, G. Zhang, *ACS Energy Lett.* **2019**, *4*, 2251.

[17] a) F. Meng, S. Bi, Z. Sun, B. Jiang, D. Wu, J. Chen, and F. Zhang, *Angew. Chem. Int. Ed.* **2021**, *60*, 13614 – 13620; b) C. Zhang, W. Cui, S. Yi, C. Niu, R. Liang, J. Qi, X. Chen, W. Jiang, X. Liu, Q. Luo, and J. Qiu, *Nat. Commun.* **2022**,*13*, 7621.

[18] a) H. Li, Q. Pan, Y. Ma, X. Guan, M. Xue, Q. Fang, Y. Yan, V. Valtchev, and S. Qiu, *J. Am. Chem. Soc.* **2016**, *138*, 14783−14788 ; b) A. Basak, S. Karak, R. Banerjee, *J. Am. Chem. Soc.* **2023**, *145*, 7592−7599; c) J. Feng, Y. Zhang, S. Ma, C. Yang, Z. Wang, S. Ding, Y. Li, and W. Wang, *J. Am. Chem. Soc.* **2022**, *144*, 6594−6603.

[19] a) H. Li, J. Ding, X. Guan, F. Chen, C. Li, L. Zhu, M. Xue, D. Yuan, V. Valtchev, Y. Yan, S. Qiu, and Q. Fang, *J. Am. Chem. Soc.* **2020**, *142*, 13334−13338; b) H. Yang, M. Hao, Y. Xie, X. Liu, Y. Liu, Z. Chen, X. Wang, G. I. N. Waterhouse, and S. Ma, *Angew. Chem. Int. Ed.* **2023**, *62*, e202303129.

[20] a) X. He, Y. Yang, H. Wu, G. He, Z. Xu, Y. Kong, L. Cao, B. Shi, Z. Zhang, C. Tongsh, K. Jiao, K. Zhu and Z. Jiang, *Adv. Mater.* **2020**, *32*, 2001284; b) M. Yang, S. Wang, Z.Liu, Y. Chen, M.J. Zaworotko, P. Cheng, J. Ma and Z. Zhang, *J. Am. Chem. Soc.* **2021**, *143*, 7732-7739.

[21] R. Wang, Z. Zhang, J. Suo, L. Liao, L. Li, Z. Yu, H. Zhang, V. Valtchev, S. Qiu, and Q. Fang, *Chem. Eng. J.* **2023**, 147403.

[22] a) J. Chang, H. Li, J. Zhao, X. Guan, C. Li, G. Yu, V. Valtchev, Y. Yan, S. Qiu and Q. Fang, *Chem. Sci.* **2021**, 8452-8457; b) F. J. Uribe-Romo, C. J. Doonan, H. Furukawa, K. Oisaki and Omar M. Yaghi, *J. Am. Chem. Soc.* **2011**, *133*, 11478–11481.

[23] S. Tao, H. Xu, Q. Xu, Y. Hijikata, Q. Jiang, S. Irle, and D. Jiang, *J. Am. Chem. Soc.* **2021**, *143*, 8970−8975.

[24] J. Yi, J. Zhang, C. Wang, N. Lv, W. Jiang, H. Liu, H. Li, W. Zhu, H. Li and H. Ji, *J. Mol. Liq.* **2021**, 117676.

[25] a) Y. Zhang, Z. Qiao, R. Zhang, Z. Wang, H. Wang, J. Zhao, D. Cao and S. Wang, *Angew. Chem. Int. Ed.* **2023**, *62*, e202314539; b) R. Khan, J. Chakraborty, K. S. Rawat, R. Morent, N. De Geyter, V. Van Speybroeck and P. Van Der Voort, *Angew. Chem. Int. Ed.* **2023**, *62*, e202313836.

[26] a) S. Huang, B. Zhang, D. Wu, Y. Xu, H. Hu, F. Duan, H. Zhu, M. Du and S. Lu, *Appl. Catal. B*, **2024**, *340*, 123216; b) Z. Yang, Y. Gao, L. Zuo, C. Long, C. Yang and X. Zhang, *ACS Catal.* **2023**, *13*, 4790−4798.

[27] a) C. Hu, R. Paul, Q. Dai and L. Dai, *Chem. Soc. Rev.* **2021**, *50*, 11785; b) N. Li, C. Huang, X. Wang, Y. Feng and J. An, *Chem. Eng. J.* 2022, *450*, 138246.

[28] Y. Wang, G. I. N. Waterhouse, L. Shang and T. Zhang, *Adv. Energy Mater.* **2021**, *11*, 2003323.

[29] J. Liu, J. Zhao, C. Li, Y. Liu, D. Li, H. Li, V. Valtchev, S. Qiu, Y. Wang and Q. Fang, *Small* **2023**, 2305759.

[30] a) M. Liu, S. Yang, S. Liu, Q. Miao, X. Yang, X. Li, Q. Xu and G. Zeng, *Small* **2022**, *18*, 2204757; b) S. Yang, L. Lu, J. Li, Q. Cheng, B. Mei, X. Li, J. Mao, P. Qiao, F. Sun, J. Ma, Q. Xu and Z. Jiang, *SusMat*. **2023**, *3*, 379–389.

[31] G. Gao, G. Zhao, G. Zhu, B. Sun, Z. Sun, S. Li, Y. Lan, *Chin. Chem. Lett.* **2024**, 109557.

[32] X. Xu, Y. Gao, Q. Yang, T. Liang, B. Luo, D. Kong, X. Li, L. Zhi and B. Wang, *Nano Today* **2023**, *49*, 101792.

[33] a) J. M. Rotter, R. Guntermann, M. Auth, A. M. ahringer, A. Sperlich, V. Dyakonov, D. D. Medina and T. Bein, *Chem. Sci.* **2020**, *11*, 12843; b) S. Xu, H. Sun, M. Addicoat, B. P. Biswal, F. He, S. Park, S. Paasch, T. Zhang, W. Sheng, E. Brunner, Y. Hou, M. Richter and X. Feng, *Adv. Mater.* **2021**, *33*, 2006274.

[34] D. W. Burke, R. R. Dasari, V. K. Sangwan, A. K. Oanta, Z. Hirani, C. E. Pelkowski, Y. Tang, R. Li, D. C. Ralph, M. C. Hersam, S. Barlow, S. Marder, and William R. Dichtel, *J. Am. Chem. Soc.* **2023**, *145*, 11969−11977.

[35] M. Fan, Z. Wang, K. Sun, A. Wang, Y. Zhao, Q. Yuan, R. Wang, J. Raj, J. Wu, J. Jiang and L. Wang, *Adv. Mater.* **2023**, *35*, 2209086.

[36] J. Zhu, X. Xiao, K. Zheng, F. Li, G. Ma, H. Yao, X. Wang and Y. Chen, *Carbon* **2019**, *153*, 6-11.

[37] a) Z. Y. Li, D. Wang, J. L. Xu, H. B. Sun, Z. N. Shi, *Chem. Eng. J.* **2024**, *482*, 148858; b) F. Zeng, C. Mebrahtu, L. F. Liao, A. K. Beine, R. Palkovits, *J. Energy Chem.* **2022**, *69*, 301.

[38] a) S. Yang, Q. Cheng, J. Mao, Q. Xu, Y. Zhang, Y. Guo, T. Tan, W. Luo, H. Yang and Z. Jiang, *Appl. Catal. B* **2021**, 298120605; b) Q. Zhi, R. Jiang, X. Yang, Y. Jin, D. Qi, K. Wang, Y. Liu, and J. Jiang, *Nat. Commun.* **2024** *15*, 678.

[39] C. Zhang, W. Shen, K. Guo, M. Xiong, J. Zhang, and X. Lu, *J. Am. Chem. Soc.* **2023**, *145*, 11589-11598.

[40] a) Z. Liu, J. Wan, Z. Yan, Y. Wang and Y. Ma, Chem. Eng. J. **2022**, *433*, 133767; b) J. Ji, Z. Wang, Q. Xu, Q. Zhu and M. Xing, *Chem. Eur. J.* **2023**, *29*, e202203921.

Entry for the Table of Contents

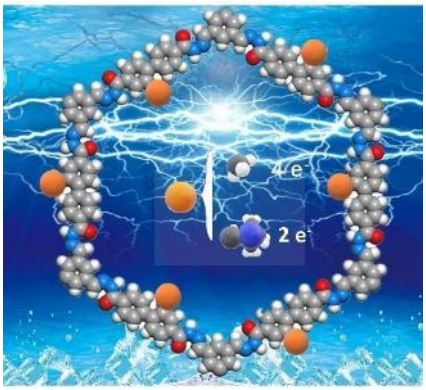

We have adeptly optimized the ORR process through strategic engineering of COFs, effectively transitioning the reaction from a four-electron pathway to a two-electron pathway. Significantly, when implemented within a flow cell apparatus, the COF augmented with ionic salt (JUC-660) demonstrated consistent productivity, maintaining a H_2O_2 yield rate in excess of 1200 mmol g^{-1} h^{-1} for an extended operational period more than 85 hours. This performance solidifies its status as one of the most efficient metal-free and non-pyrolyzed catalysts reported to date.